MHD BOUNDARY LAYER SLIP FLOW OF A CASSON FLUID OVER AN EXPONENTIALLY STRETCHING SURFACE IN THE PRESENCE OF THERMAL RADIATION AND CHEMICAL REACTION

P. Bala Anki Reddy

Department of Mathematics, School of Advanced Sciences, VIT University, Vellore, T.N.-632014. E-mail: pbarmaths@gmail.com, sireesha.siri7@gmail.com

Abstract:

An analysis is carried out to investigate the steady two-dimensional magnetohydrodynamic boundary layer flow of a Casson fluid over an exponentially stretching surface in the presence of thermal radiation and chemical reaction. Velocity, thermal and solutal slips are considered instead of no-slip conditions at the boundary. Stretching velocity, wall temperature and wall concentration are considered in the exponential forms. The non-linear partial differential equations are converted into a system of non-linear ordinary differential equations by similarity transformations. The resultant non-linear ordinary differential equations are solved numerically by fourth order Runge-Kutta method along with shooting technique. The influence of various parameters on the fluid velocity, temperature, concentration, wall skin friction coefficient, the heat transfer coefficient and the Sherwood number have been computed and the results are presented graphically and discussed quantitatively. Comparisons with previously published works are performed on various special cases and are found to be in excellent agreement.

Keywords: Exponentially stretching surface, Casson fluid, MHD, thermal radiation, chemical reaction, suction/blowing.

1. Introduction

Investigations on the boundary layer flows of Newtonian fluids over a stretching surface have gained considerable attention because of its wide range of applications in technology and industry. Such applications include polymer extrusion from a dye, wire drawing, the boundary layer along a liquid film in condensation processes, accelerators, paper production, artificial fibers, hot rolling, glass blowing, cooling of metallic sheets or electronic chips, metal spinning, drawing plastic films and many others. Crane (1970) pioneered a closed form analytical solution for an incompressible fluid flow due to a linearly stretching sheet. Many researchers (Bidin and Nazar, 2009; Magyari and Keller, 200; Mukhopadhyay and Reddy, 2012; Misra and Sinha, 2013; Fang et al., 2009; Aziz, 2009; Srinivas et al., 2014; Nadeem et al., 2011; Reddy and Reddy, 2011 and Ishak, 2011) extended the work of crane by considering several physical aspects taking Newtonian fluid. But in real life, some materials like, melts muds, condensed milk, glues, printing ink, emulsions, tomato paste, paints, soaps, shampoos, sugar solution, etc. shows different characters which are not properly understandable using Newtonian theory. Therefore, the analysis of non-Newtonian fluid flows is an essential part in the study of fluid dynamics and heat and mass transfer. Constitutive equations are used for the Casson fluid. Casson fluid is one of the non-Newtonian fluids which exhibits yield stress. However such fluids behaves like a solid when shear stress less than the yield stress is applied and it moves if applied shear stress is greater than yield stress. Examples of Casson fluid model jelly, soup, honey, tomato sauce, concentrated fruit juices and many others. Human blood is also a Casson fluid. In fact because of several substances like protein, fibrinogen and globin in aqueous base plasma, human red cells from a chain like structure, known as aggregates or rouleaux. If the rouleaux behave like a plastic solid then there exists a field stress that can be identified with the constant stress in Casson fluid. This fluid can be defined as a shear thinning liquid having infinite viscosity at zero shear rate, a yield stress below which no flow occurs and a zero viscosity at an infinite shear rate was examined by Dash et al (1996). Several studies (Nadeem et al., 2012; Nadeem et al., 2014; Hayat et al., 2012, Mukhopadhyay et al., 2013; Mustafa et al., 2012; Bhattacharya et al., 2013 and Mustafa. 2011) have been reported investigating the Casson fluid flow over a stretching surface. Bhattacharya et al. (2014) studied the boundary layer flow of Casson fluid over a stretching/shrinking sheet. Numerical solutions for the steady boundary layer Cason fluid flow and heat transfer passing a nonlinearly stretching surface was studied by Mukhopadhyay (2013). Recently, the numerical solutions for steady boundary layer flow and heat transfer for a Casson fluid over an exponentially permeable stretching surface in the presence of thermal radiation are analyzed by Pramanik (2014). Very recently, the steady two-dimensional MHD convective boundary layer flow of a Casson fluid over an

exponentially inclined permeable stretching surface in the presence of thermal radiation and chemical reaction was discussed by Reddy (2016).

To the best of author's knowledge, no investigation has been made yet to analyze the steady two-dimensional boundary layer flow of a Casson fluid over an exponentially stretching surface in the presence of thermal radiation and chemical reaction. The present work aims to fulfill the gap in the existing literature. Motivated by the above studies, a mathematical model is presented here to understand the effects of thermal radiation and chemical reaction on the steady two-dimensional boundary layer flow of a Casson fluid over an exponentially stretching surface. The governing partial differential equations of the governing flow are transformed into non-linear coupled ordinary differential equations by a Similarity transformation. The resulting nonlinear coupled differential equations are solved numerically by using fourth order Runge-Kutta scheme together with shooting method and the flow characteristics are analysed with the help of their graphical representations.

2. Mathematical Formulation:

Consider two-dimensional flow of an incompressible viscous electrically conducting Casson fluid over an exponentially stretching surface coinciding with the plane $y = 0$. The x-axis is taken along the stretching surface in the direction of the motion while the y-axis is perpendicular to the surface. The flow is confined to $y > 0$. Two equal and opposite forces are applied along the x-axis so that the wall is stretched keeping the origin fixed. The coordinate system and flow model are shown in Fig.1.
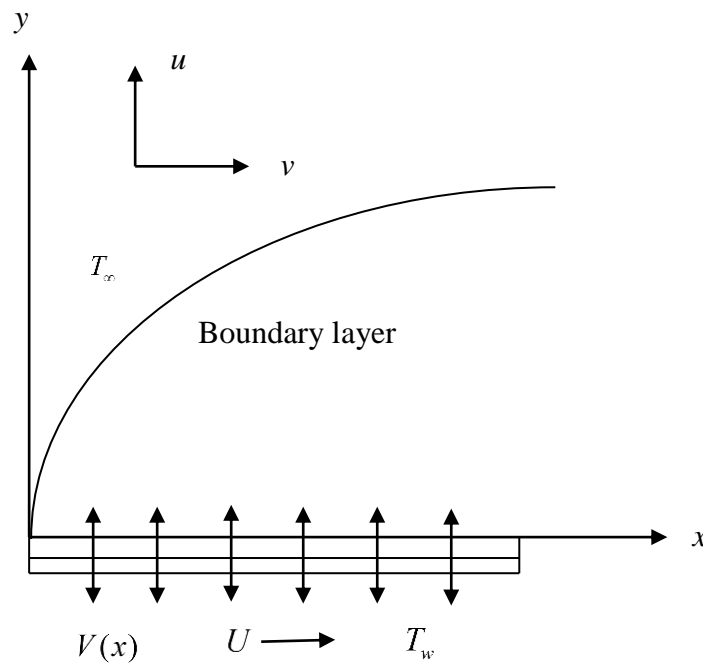

Fig. 1: Sketch of the physical flow problem

A variable magnetic field $B = B_0 e^{\frac{x}{2L}}$ is applied normal to the sheet, B_0 is a constant. Assume that the rheological equation of state for an isotropic and incompressible flow of a Casson fluid is as follows: (Mukhopadhyay, 2013 and Mukhopadhyay et al., 2013)

$$\tau_{ij} = \begin{cases} 2\left(\mu_B + {P_y}\big/{\sqrt{2\pi}}\right)e_{ij}, & \pi > \pi_c \\ 2\left(\mu_B + {P_y}\big/{\sqrt{2\pi_c}}\right)e_{ij}, & \pi < \pi_c \end{cases}$$

where μ_B is the plastic dynamic viscosity of the non-Newtonian fluid, P_y is the yield stress of the fluid, $\pi = e_{ij}e_{ij}$, e_{ij} is the $(i, j)^{th}$ component of the deformation rate and π_c is the critical value of this product based on the non-Newtonian model. Under these assumptions, the governing boundary layer along with the Boussinesq approximation, the continuity, momentum, energy and concentration species can be written as

$$\frac{\partial u}{\partial x} + \frac{\partial v}{\partial y} = 0 \tag{1}$$

$$u\frac{\partial u}{\partial x} + v\frac{\partial u}{\partial y} = \upsilon\left(1 + \frac{1}{\beta}\right)\frac{\partial^2 u}{\partial y^2} - \frac{\sigma B^2}{\rho}u \tag{2}$$

$$u\frac{\partial T}{\partial x} + v\frac{\partial T}{\partial y} = \frac{k}{\rho c_p}\frac{\partial^2 T}{\partial y^2} - \frac{1}{\rho c_p}\frac{\partial q_r}{\partial y} \tag{3}$$

$$u\frac{\partial C}{\partial x} + v\frac{\partial C}{\partial y} = D\frac{\partial^2 C}{\partial y^2} - \Gamma\left(C - C_\infty\right) \tag{4}$$

Subject to the boundary conditions:

$$u = U + N\mu\frac{\partial u}{\partial y}, v = -V(x), T = T_w + M\frac{\partial T}{\partial y}, C = C_w + P\frac{\partial C}{\partial y} \text{ at } y = 0$$

$$u \to 0, T \to T_\infty, C \to C_\infty \text{ as } y \to \infty \tag{5}$$

Here $U = U_0 e^{\frac{x}{L}}$ is the stretching velocity, $T_w = T_\infty + T_0 e^{\frac{x}{L}}$ is the temperature at the sheet, $C_w = C_\infty + C_0 e^{\frac{x}{L}}$ is concentration at the sheet, U_0, T_0 and C_0 are the reference velocity, temperature and concentration respectively, $N = N_1 e^{\frac{-x}{L}}$ is the velocity slip factor, $M = M_1 e^{\frac{-x}{L}}$ is the thermal slip factor and $P = P_1 e^{\frac{-x}{L}}$ is the solutal slip factor. The no-slip conditions can be recovered, by setting $N = M = P = 0$. $V(x) = V_0 e^{\frac{x}{2L}}$ a special case of velocity at the wall considered, $V(x) > 0$ be the velocity of suction and $V(x) < 0$ be the velocity of blowing. It is assumed that the exponential reaction rate is in the form of $\Gamma = k_0 e^{\frac{x}{L}}$. Where u and v are the velocity components in the x and y directions respectively, ρ is the density of the fluid, υ is the kinematic viscosity, β is the Casson parameter, T is the temperature, T_∞ is the temperature of the ambient fluid, C is the concentration, C_∞ is the concentration of the ambient fluid, σ is the electrical conductivity, υ is the kinematic viscosity, c_p is the specific heat at constant pressure, k is the thermal conductivity, q_r is the radiative heat flux, D is the mass diffusion coefficient and L is the reference length. In (5), U is a constant with $U > 0$ for stretching and $U < 0$ for shrinking sheet. The subscript w denotes the values at the solid surface. Furthermore, N, M and P represents the velocity, thermal and solutal slip factors respectively and when $L = K = P = 0$, the slip condition is recovered.

Thermal radiation is simulated using the Rosseland diffusion approximation and in accordance with this, the radiative heat flux q_r is given by

$$q_r = -\frac{4\sigma^*}{3k^*}\frac{\partial T^4}{\partial y} \tag{6}$$

Where σ^* is the Stefan–Boltzmann constant and k^* is the Rosseland mean absorption coefficient. If the temperature differences within the mass of blood flow are sufficiently small, then Equation (6) can be linearized by expanding T^4 into the Taylor's series about T_∞ and neglecting higher order terms, we get

$$T^4 \cong 4T_\infty^3 T - 3T_\infty^4 \tag{7}$$

Invoking Equations (6) and (7), Equation (3) can be written as

$$u\frac{\partial T}{\partial x} + v\frac{\partial T}{\partial y} = \left(\frac{k}{\rho c_p} + \frac{16T_\infty^3}{3\rho C_p k^*}\right)\frac{\partial^2 T}{\partial y^2} \tag{8}$$

We introduce the similarity variables as

$$\eta = \left(\frac{U_0}{2\upsilon L}\right)^{\frac{1}{2}} e^{\frac{x}{2L}} y, \ u = U_0 e^{\frac{x}{L}} f'(\eta), v = -\sqrt{\frac{\upsilon U_0}{2L}} e^{\frac{x}{2L}} \left(f(\eta) + \eta f'(\eta)\right), \ T = T_\infty + T_0 e^{\frac{x}{2L}} \theta(\eta),$$

$$C = C_\infty + C_0 e^{\frac{x}{2L}} \phi(\eta) \tag{9}$$

where η is the similarity variable.

Now substituting (9) into the Eqs. (2), (4) and (8), we get the following set of ordinary differential equations

$$\left(1 + \frac{1}{\beta}\right) f''' + f f'' - 2(f')^2 - Hf' = 0 \tag{10}$$

$$\left(1 + \frac{4}{3}R\right)\theta'' + \Pr(f\theta' - f'\theta) = 0 \tag{11}$$

$$\phi'' + Sc(f\phi' - f'\phi) - Sc\gamma\phi = 0 \tag{12}$$

with the boundary conditions

$$f = S, f' = 1 + S_f f''(0), \ \theta = 1 + S_t \theta'(0), \ \phi = 1 + S_c \phi'(0) \quad \text{at } \eta = 0$$

$$f' \to 0, \ \theta \to 0, \ \phi \to 0 \text{ as } \eta \to \infty \tag{13}$$

where H, R, $\Pr$, Sc, γ and S are non-dimensional parameters called respectively the dimensionless magnetic parameter, radiation parameter, Prandtl number, Schmidt number, chemical reaction parameter and suction parameter are given by

$$H = \frac{2B^2 L}{\rho U_0}, \ R = \frac{4\sigma^* T_\infty^3}{kk^*}, \ \Pr = \frac{\mu c_p}{k}, \ Sc = \frac{\upsilon}{D}, \gamma = \frac{2Lk_0}{U_0} \text{ and } S = \frac{V_0}{\sqrt{\frac{U_0\upsilon}{2L}}} \tag{14}$$

In Eq. (13), $S < 0$ and $S > 0$ correspond to injection and suction respectively. The non-dimensional velocity slip S_f, thermal slip S_t and solutal slip S_c are defined by

$$S_f = N_1\rho\sqrt{\frac{\upsilon U_0}{2L}}, S_t = M_1\sqrt{\frac{U_0}{2\upsilon L}} \text{ and } S_c = P_1\sqrt{\frac{U_0}{2\upsilon L}} \ . \tag{15}$$

The quantities of physical interest in this problem are the skin-friction coefficient, heat transfer rate and mass transfer, which are defined as

$$C_f = \frac{2\tau_w}{\rho U_0^2 e^{\frac{2x}{L}}}, Nu_x = \frac{xq_w}{k(T_w - T_\infty)} \text{ and } Sh_x = \frac{xJ_w}{D(C_w - C_\infty)} \tag{16}$$

Respectively, where the surface shear stress τ_w, surface heat flux q_w and mass flux J_w are given by

$$\tau_w = \mu\left(\frac{\partial u}{\partial y}\right)_{y=0}, \ q_w = -k\left(\frac{\partial T}{\partial y}\right)_{y=0} \text{ and } J_w = -D\left(\frac{\partial C}{\partial y}\right)_{y=0} \tag{17}$$

Substituting (9) and (17) into Equations. (16) give

$$C_f\sqrt{\Re_x / 2} = f''(0), \ \frac{Nu_x}{\sqrt{\Re_x/2}\sqrt{x/L}} = -\theta'(0) \text{ and } \frac{Sh_x}{\sqrt{\Re_x/2}\sqrt{x/L}} = -\phi'(0) \tag{18}$$

where $\mathrm{Re}_x = \dfrac{xU_0 e^{\frac{x}{L}}}{\upsilon}$ is the local Reynolds number. The above Skin-friction coefficient, local Nusselt number and Sherwood number shows that its variation depends on the variation of the factors $f''(0)$, $-\theta'(0)$ and $-\phi'(0)$ respectively.

3. Numerical Method for Solution:

The set of nonlinear coupled differential equations (10)-(12) subject to the boundary conditions (13) are solved using shooting method, by converting them to an initial value problem. We set

$f' = z, z' = p,$

$$\mathrm{p}' = \left(\frac{\beta}{1+\beta}\right)(2z^2 - fp + Hz) \tag{19}$$

$$\theta' = q, q' = -\left(\frac{3\mathrm{Pr}}{4R+3}\right)(fq - z\theta) \tag{20}$$

$$\phi' = r, r' = -sc(fr - z\phi + \gamma\phi) \tag{21}$$

with the boundary conditions

$$f(0) = s, f'(0) = 1 + s_f\alpha, \alpha = f''(0), \theta(0) = 1 + \mathrm{s}_t\beta, \beta = \theta'(0), \phi(0) = 1 + \mathrm{s}_c\delta, \delta = \phi'(0). \tag{22}$$

In order to integrate Eqns.(19)-(21) as an initial value problem one requires a value for $p(0)$ i.e., $f''(0)$, $q(0)$ i.e., $\theta'(0)$ and $r(0)$ i.e., $\phi'(0)$ but no such values are given at the boundary. The suitable guess values for $f''(0)$, $\theta'(0)$ and $\phi'(0)$ are chosen and the fourth order Runge-Kutta method with step size 0.01 is applied to obtain the solution.

4. Results and Discussion

In the present study to gain a physical insight into the problem, velocity, temperature and concentration distributions have been discussed by assigning numerical values to various parameters obtained in the mathematical formulation of the problem and the numerical results are shown graphically. The default values of the various parameters which we considered were β = 2.0, H = 1.0, R = 0.5, Pr = 0.72, Sc = 0.60, $\gamma = 0.5$, $S_f = 0.5$, $S_t = 0.5$, $S_c = 0.5$ and S = 0.5 unless otherwise specified. In order to check the accuracy and validity of the applied numerical scheme, comparisons of the present numerical results corresponding to the heat transfer coefficient for various values of Prandtl number and thermal radiation in the absence of Casson fluid parameter, magnetic parameter, thermal radiation, Schmidt number, suction parameter, velocity slip, thermal slip and solutal slip with the available published results of Bidin and Nazar (2009), Magyari and Keller (2000), Mukhopadhyay and Reddy (2012), Ishak (2011), Nadeem et al. (2011) and Pramanik (2014) are made (see Table 1 and Table 2) and are found to be in excellent agreement.

Table 1: Comparison $-\theta'(0)$ for several values of Prandtl number in the absence of Casson fluid parameter, magnetic parameter, thermal radiation, Schmidt number, suction parameter, velocity slip, thermal slip and solutal slip.

Pr	Bidin and Nazar (2009)	Magyari and Keller (2000)	El-Aziz (2009)	Ishak (2011)	Pramanik (2014)	Present
1	0.9547	0.95478	0.9548	0.9548	0.9547	0.95477
2	1.4714			1.4715	1.4714	1.47144
3	1.8691	1.8691	1.8691	1.8691	1.8691	1.86916
5		2.5001	2.5001	2.5001	2.5001	2.50016
10		3.6604	3.6604	3.6604	3.6604	3.66038

Table 2: Comparison $-\theta'(0)$ for several values of Prandtl number and thermal radiation parameter in the absence of Casson fluid parameter, magnetic parameter, Schmidt number, suction parameter, velocity slip, thermal slip and solutal slip.

	Bidin and Nazar (2009)		Nadeem et al. (2011)		Pramanik (2014)		Present	
Pr	0.5	1	0.5	1	0.5	1	0.5	1
1	0.6765	0.5315	0.680	0.534	0.6765	0.5315	0.6765	0.5315
2	1.0735	0.8627	1.073	0.863	1.0734	0.8626	1.0734	0.8627
3	1.3807	1.1214	1.381	1.121	1.3807	1.1213	1.3807	1.1213

The velocity, temperature and concentration for different values of Casson fluid parameter, magnetic parameter, velocity slip, thermal radiation parameter, Prandtl number, thermal slip, Schmidt number, solutal slip and chemical reaction for both cases of suction and blowing are shown graphically in Figs. 2-11. The effects of the Casson fluid parameter on the velocity, velocity gradient, temperature, temperature gradient, concentration and concentration gradient profiles in the presence of suction/blowing are exhibited in Figs. 2(a)-(f) respectively. From Fig. 2(a), we observed that, the velocity and the momentum boundary layer thickness decreases with the increase of Casson fluid parameter for both the cases of suction and blowing. It is found that the magnitude of shear stress decreases initially with the Casson fluid parameter but increases significantly after a certain distance η normal to the sheet (Fig. 2(b)). Fig. 2(c), it is very clear that, the temperature and the thermal boundary layer thickness increases as the Casson fluid parameter increases for both the cases of suction and blowing. The variations in the temperature gradient for changes in the Casson fluid parameter are presented in Fig. 2(d). It is noticed that the temperature gradient increases initially but it decreases after a certain distance η normal to the sheet. The effect of the Casson fluid parameter on the concentration is presented in Fig. 2(e). It can be observed that an increase in the Casson fluid parameter enhances the concentration profiles. From Fig. 2(f), it is noticed that the concentration gradient increases initially but it decreases after a certain distance η normal to the sheet. Figs. 3(a)-(d) focus on the velocity, velocity gradient, temperature and concentration distributions for various values of the magnetic parameter. Fig. 3(a) represents the velocity profiles for various values of magnetic parameter in the boundary layer for suction and blowing cases. From this figure it can be seen that the velocity and the momentum boundary layer thickness reduces with increasing values of magnetic parameter. This is due to the fact that an increase in magnetic parameter signifies an enhancement of Lorentz force, thereby reducing the magnitude of the velocity. Fig. 3(b) is aimed to shed light on the effect of magnetic parameter on the velocity gradient distribution. It can be noticed from this figure that the velocity gradient distribution of the flow field reduces as the magnetic parameter increases. The variations in the temperature profiles for changes in the magnetic parameter are presented in Fig. 3(c) for suction and blowing cases. It is observed that the temperature profiles and the thermal boundary layer thickness increases with an increase in the magnetic parameter. Fig. 3(d) describes the variation of concentration distribution for different values of magnetic parameter for suction and blowing cases. It is found that an increase in the magnetic parameter enhances concentration gradient for the suction and blowing cases. Figs. 4(a)–(b) depict the influence of velocity and the velocity gradient for different values of velocity slip. The variations in the velocity profiles for changes in the velocity slip are presented in Fig. 4(a). It can be noticed that the velocity of the boundary layer reduces with increasing values of velocity slip parameter for suction and blowing cases. Fig. 4(b) displays the variations of velocity gradient profile with changes in the dimensionless velocity slip for suction and blowing cases. Results indicate that the increase in the Velocity slip enhances the velocity.

Figs. 5(a)-(b) focus on the temperature and temperature gradient for various values of the thermal radiation parameter. Fig. 5(a) represents the temperature profiles for various values of thermal radiation parameter in the boundary layer for suction and blowing. From this it can be inferred that an increase in the thermal radiation enhances the heat transfer. Fig. 5(b) is aimed to shed light on the effect of thermal radiation parameter on the temperature gradient distribution. It is noticed that the temperature gradient increases initially but it decreases after a certain distance η normal to the sheet. Fig. 6(a) describes the variation of temperature distribution for different values of Prandtl number for the suction and blowing. From this plot, it is evident that the thickness of the boundary layer as well as the temperature profiles decreases with an increase in the value of the Prandtl number. The changes in the temperature gradient profiles for various values of Prandtl number is plotted in Fig. 6(b). It is noticed that the temperature gradient decrease initially but it increases after a certain distance η normal to the sheet. The variations in the temperature profiles for changes in the thermal slip are presented in Fig. 7(a) for the suction and blowing. From this figure it can be seen that the temperature of the boundary layer

reduces with increasing values of thermal slip parameter. Fig. 7(b) represents the temperature gradient profiles for various values of thermal slip. It can be inferred that an increase in the thermal slip parameter enhances temperature gradient for the suction and blowing cases. Fig. 8(a) demonstrates the effect of the Schmidt number on the concentration distribution. One can observe that the concentration distribution of the flow field reduces as the Schmidt number increases for the suction and blowing cases. Fig. 8(b) is a plot of concentration gradient distribution for various values of Schmidt number for the suction and blowing. It is observed that the concentration gradient decreases initially but it increases after a certain distance η normal to the sheet. Fig. 9(a) shows that the concentration decreases with the increase of solutal slip for suction and blowing. We noticed from the Fig. 9(b) that the concentration gradient profiles increase with an increase in the solutal slip. Figs. 10(a)-(b) shows the influence of the chemical reaction on the concentration and the concentration gradient profiles in the boundary layer for the case of suction. It reveals that the concentration decreases with an increase in the destructive ($\gamma > 0$) chemical reaction, whereas the reverse trend is observed in the case of generative ($\gamma < 0$) chemical reaction (Fig. 10(a)). From the Fig. 10(b), it is observed that the concentration gradient decreases with an increase in the destructive ($\gamma > 0$) chemical reaction, whereas the reverse trend is observed in the case of generative ($\gamma < 0$) chemical reaction. Figs. 11(a)-(b) focus the influence of the chemical reaction on the concentration and the concentration gradient profiles in the boundary layer for the case of blowing. It can be seen that the concentration decreases with an increase in the destructive ($\gamma > 0$) chemical reaction, whereas the reverse trend is observed in the case of generative ($\gamma < 0$) chemical reaction (Fig. 11(a)). From the Fig. 11(b), it is noticed that the concentration gradient decreases with an increase in the destructive ($\gamma > 0$) chemical reaction, whereas the reverse trend is observed in the case of generative ($\gamma < 0$) chemical reaction.
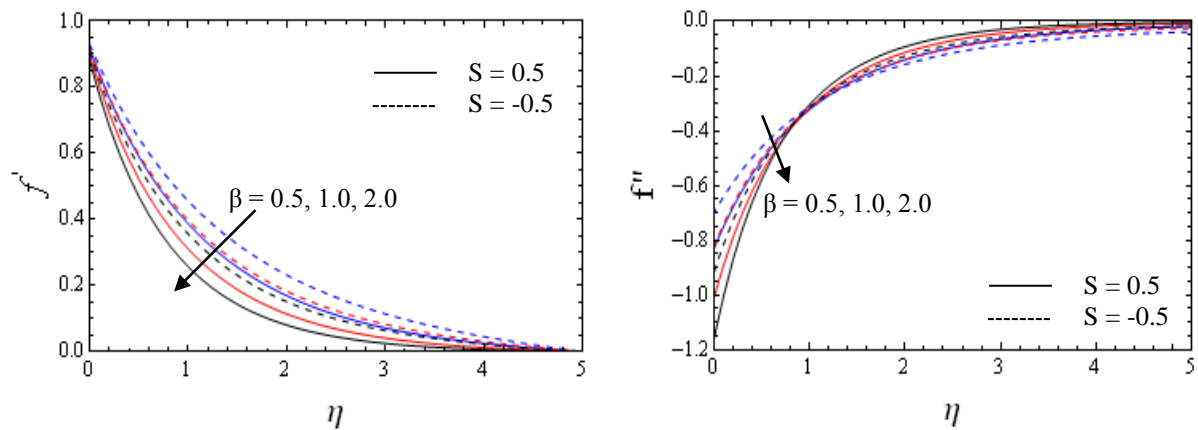

Fig. 2: (a) Velocity profiles for several values of Casson parameter of suction/blowing

(b) Velocity gradient profiles for several values of Casson parameter of suction/blowing
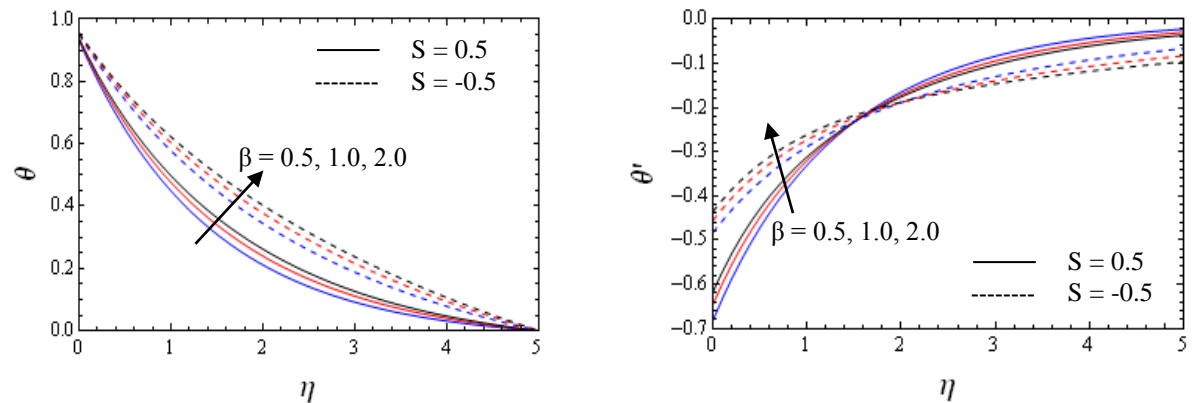
Fig. 2: (c) Temperature profiles for several values of Casson parameter of suction/blowing

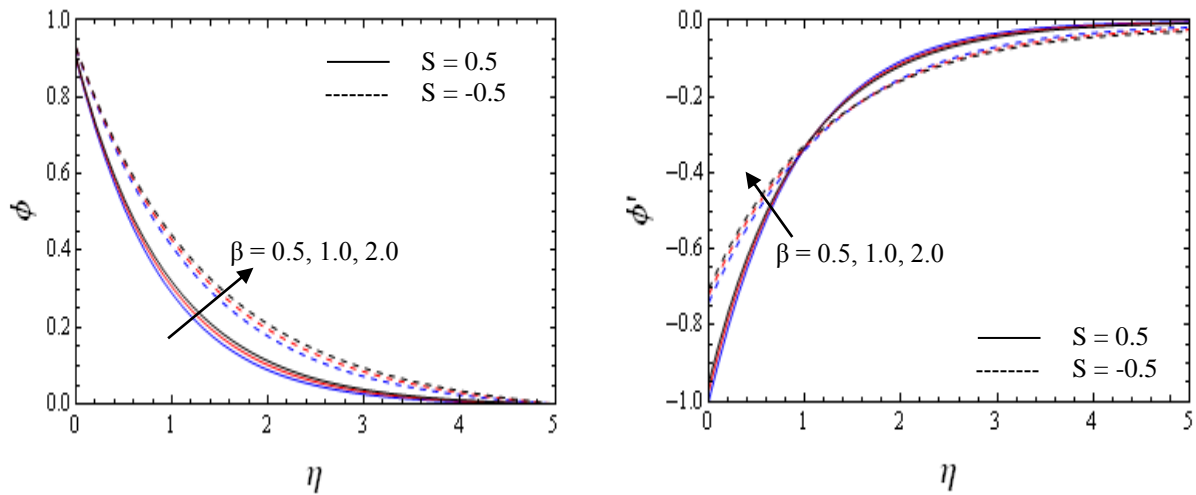(d) Temperature gradient profiles for several values of Casson parameter of suction/blowing

Fig. 2: (e) Concentration profiles for several values of Casson parameter of suction/blowing

(f) Concentration gradient profiles for several values of Casson parameter of suction/blowing
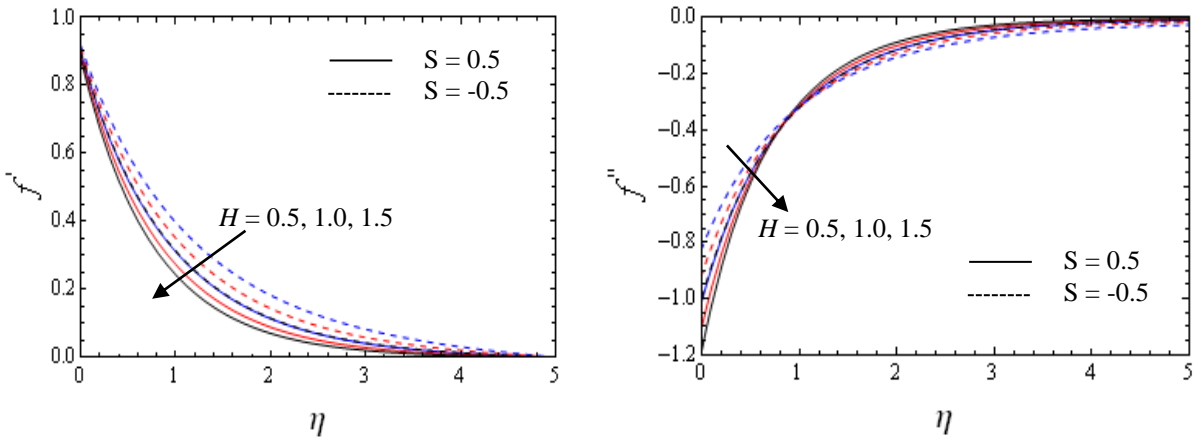

Fig. 3: (a) Velocity profiles for several values of magnetic parameter of suction/blowing

(b) Velocity gradient profiles for several values of magnetic parameter of suction/blowing
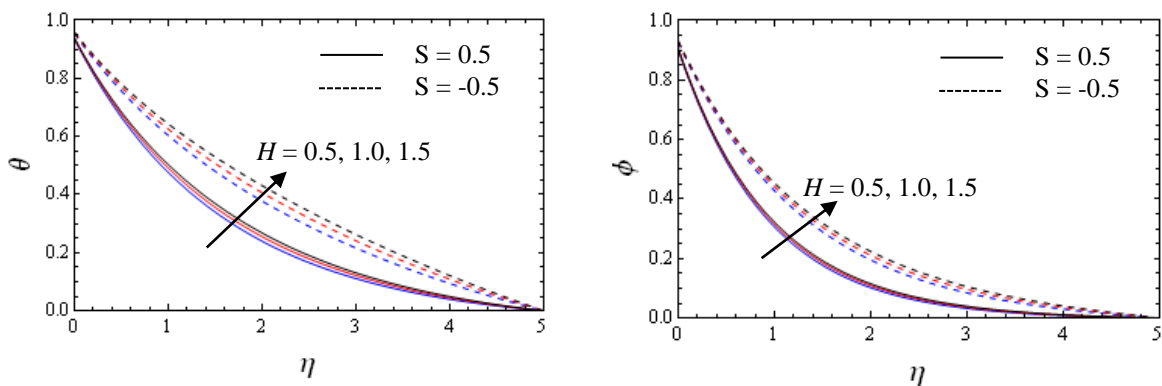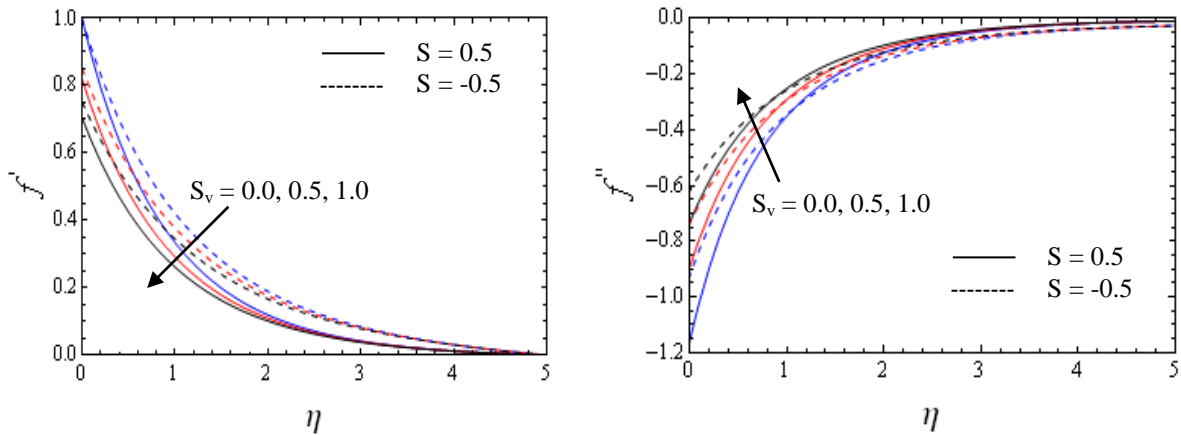

Fig. 3: (c) Temperature profiles for several values of magnetic parameter of suction/blowing

(d) Concentration profiles for several values of magnetic parameter of suction/blowing

Fig. 4: (a) Velocity profiles for several values of velocity slip of suction/blowing

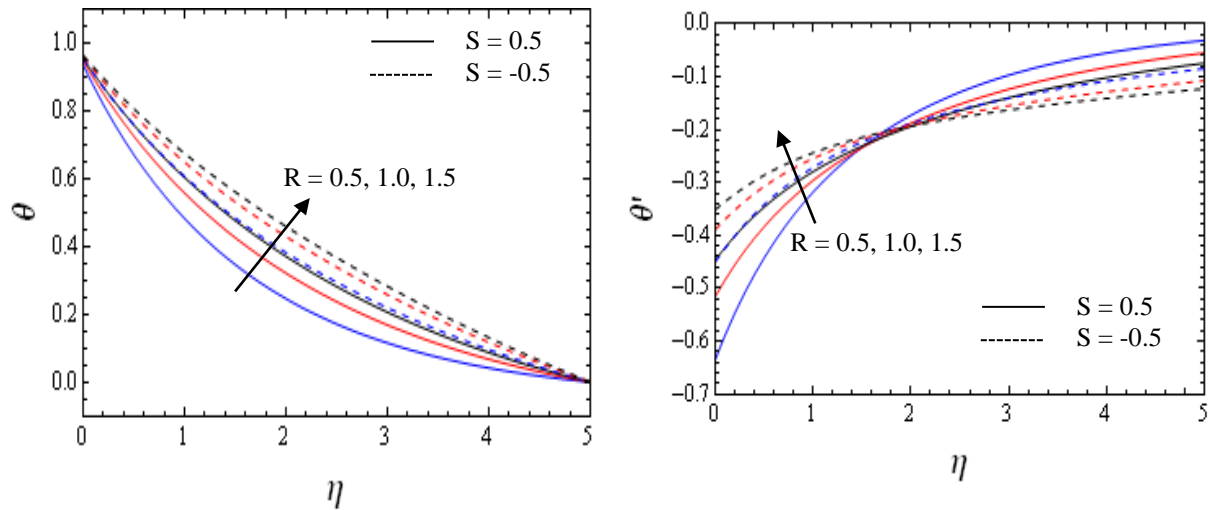(b) Velocity gradient profiles for several values of velocity slip of suction/blowing

Fig. 5: (a) Temperature profiles for several values of radiation parameter of suction/blowing

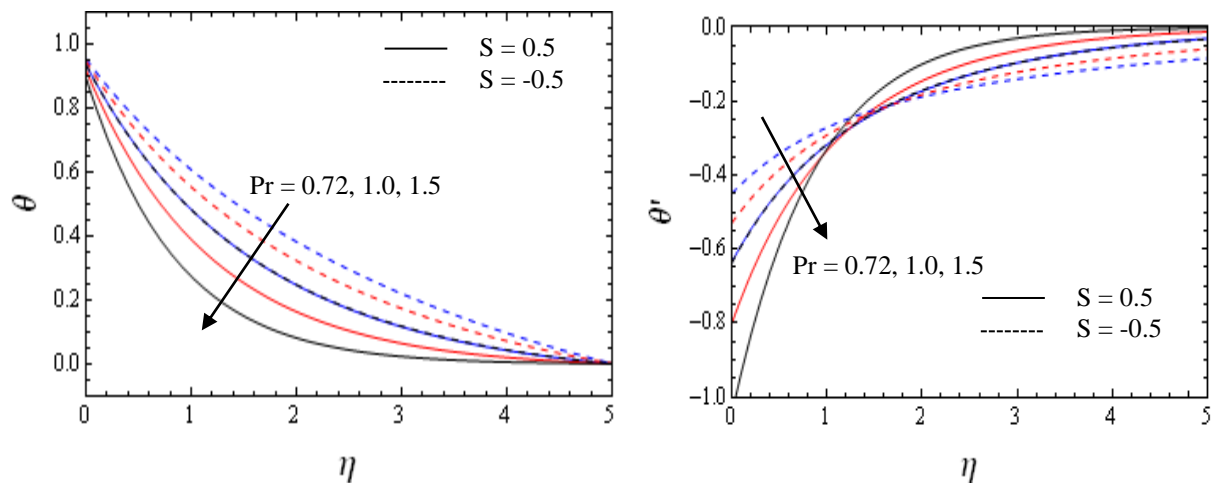(b) Temperature gradient profiles for several values of radiation parameter of suction/blowing

Fig. 6: (a) Temperature profiles for several values of Prandtl number of suction/blowing

(b) Temperature gradient profiles for several values of Prandtl number of suction/blowing
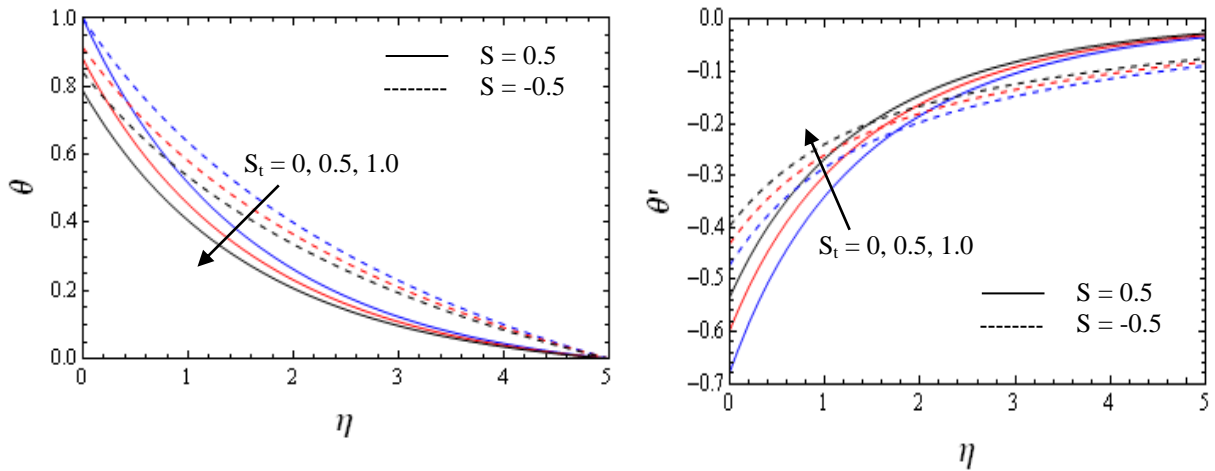
Fig. 7: (a) Temperature profiles for several values of thermal slip of suction/blowing

(b) Temperature gradient profiles for several values of thermal slip of suction/blowing
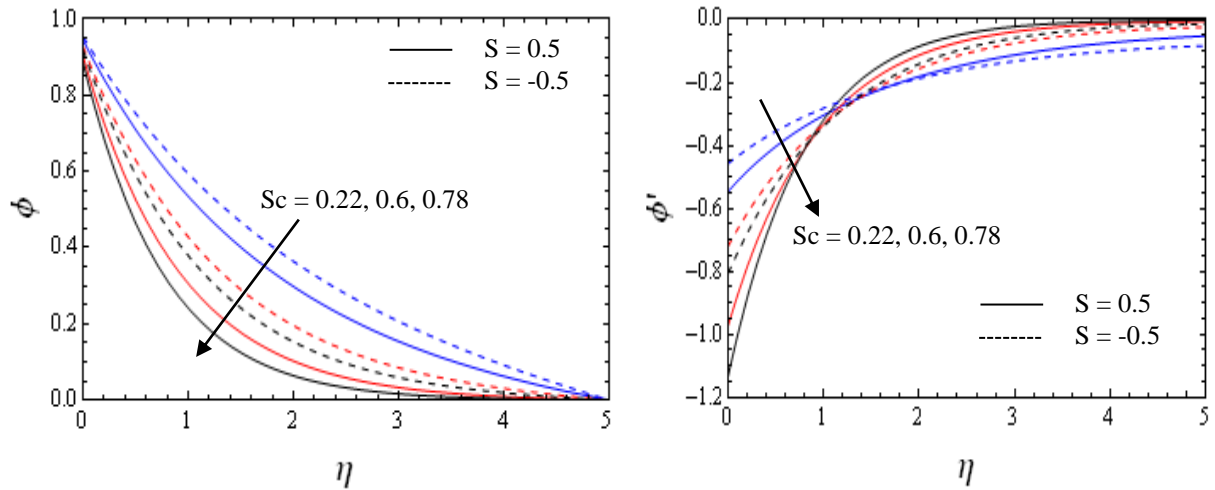

Fig. 8: (a) Concentration profiles for several values of Schmidt number of suction/blowing

(b) Concentration gradient profiles for several values of Schmidt number of suction/blowing
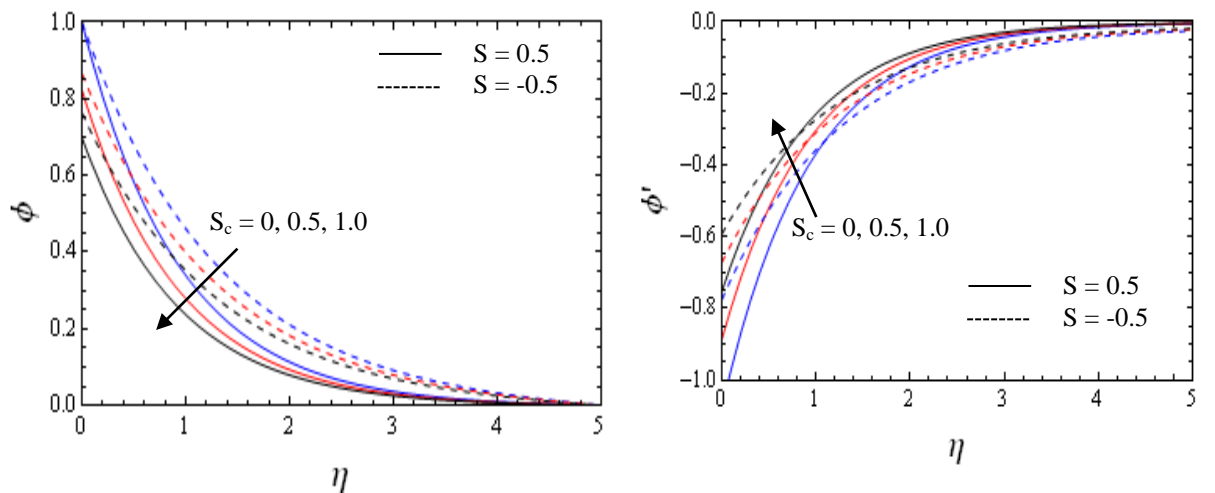

Fig. 9: (a) Concentration profiles for several values of Solutal slip of suction/blowing

(b) Concentration gradient profiles for several values of Solutal slip of suction/blowing
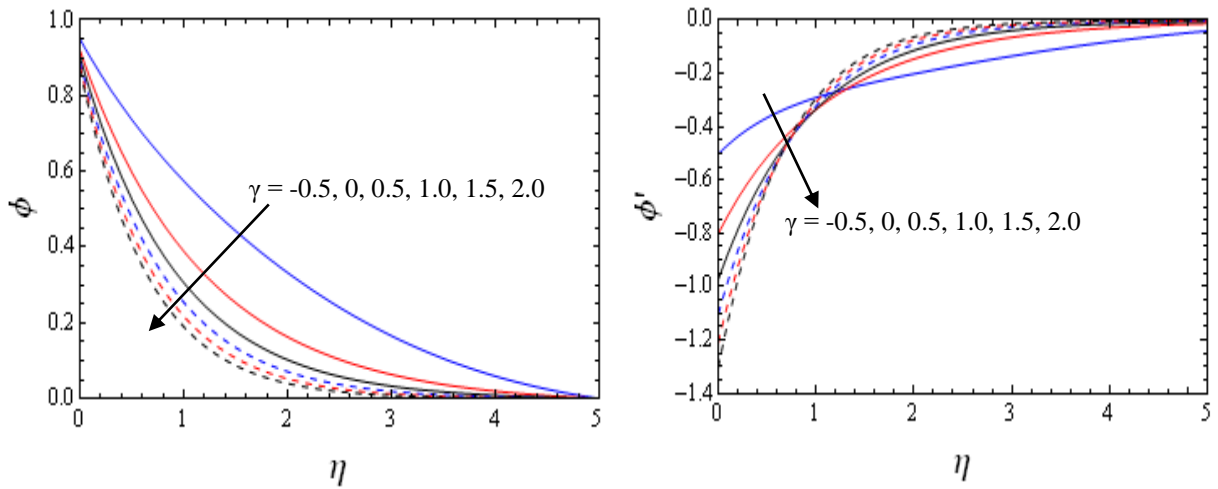
Fig. 10: (a) Concentration profiles for several values of chemical reaction parameter of suction

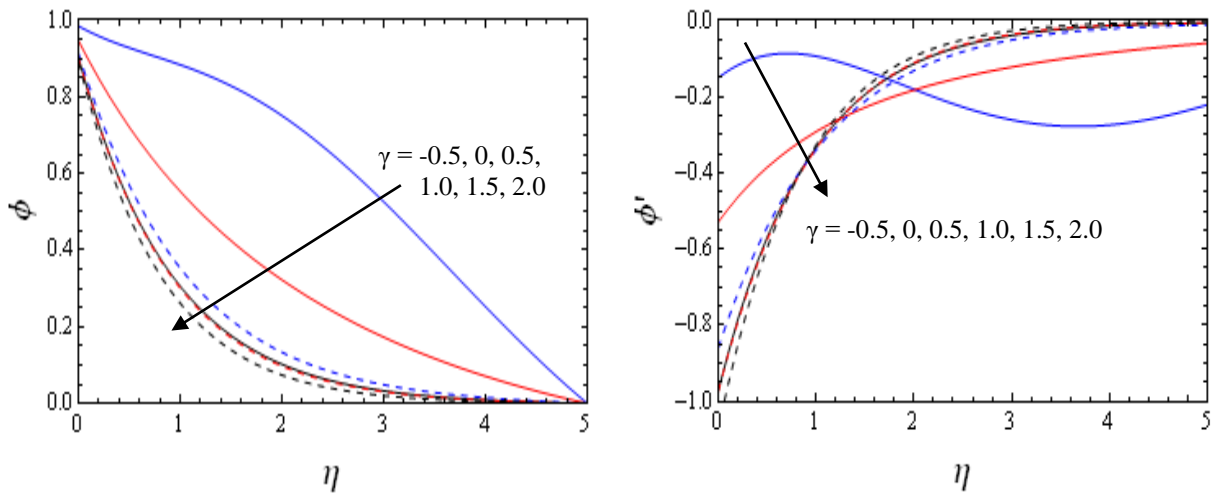(b) Concentration gradient profiles for several values of chemical reaction parameter of suction

Fig. 11: (a) Concentration profiles for several values of chemical reaction parameter of blowing

(b) Concentration gradient profiles for several values of chemical reaction parameter of blowing

Table 3: The values of skin friction coefficient, Sherwood number and the Nusselt number for various values of H, S_f, R, Pr, S_t, Sc, γ, S_c and S.

β	H	S_f	R	Pr	S_t	Sc	γ	S_c	S	$f''(0)$	$-\theta'(0)$	$-\phi'(0)$
2.0	0.5	0.5	0.5	0.7	0.5	0.6	0.5	0.5	0.5	-0.84779	0.43524	0.63787
3.0	0.5	0.5	0.5	0.7	0.5	0.6	0.5	0.5	0.5	-0.90234	0.42431	0.61722
2.0	1.0	0.5	0.5	0.7	0.5	0.6	0.5	0.5	0.5	-0.90317	0.42195	0.62803
2.0	0.5	1.0	0.5	0.7	0.5	0.6	0.5	0.5	0.5	-0.57730	0.40871	0.61514
2.0	0.5	0.5	1.0	0.7	0.5	0.6	0.5	0.5	0.5	-0.84779	0.37775	0.63787
2.0	0.5	0.5	0.5	1.0	0.5	0.6	0.5	0.5	0.5	-0.84779	0.51543	0.63787
2.0	0.5	0.5	0.5	0.7	1.0	0.6	0.5	0.5	0.5	-0.84779	0.35745	0.63787
2.0	0.5	0.5	0.5	0.7	0.5	1.0	0.5	0.5	0.5	-0.84779	0.43524	0.48362
2.0	0.5	0.5	0.5	0.7	0.5	0.6	1.0	0.5	0.5	-0.84779	0.43524	0.71746
2.0	0.5	0.5	0.5	0.7	0.5	0.6	0.5	1.0	0.5	-0.84779	0.43524	0.48362
2.0	0.5	0.5	0.5	0.7	0.5	0.6	0.5	0.5	1.0	-0.93642	0.50393	0.71383

5. Conclusions

A numerical study is performed to analyze the boundary layer Casson fluid flow over an exponentially stretching sheet in the presence of slips, thermal radiation and chemical reaction. The governing partial differential equations have been transformed by a similarity transformation into a system of ordinary differential equations, which are solved numerically using the Runge–Kutta fourth order along with a shooting technique. The main numerical results of the present analysis can be listed as follows:

(i) Momentum boundary layer thickness decreases with an increasing the Casson fluid parameter, whereas the reverse trend for the thermal boundary layer thickness. Also the same trend is observed in the case of magnetic parameter.
(ii) The temperature increases with an increasing the radiation parameter, whereas the reverse trend is observed in the case of Prandtl number.
(iii) The concentration decreases with an increase in the destructive chemical reaction, whereas the reverse trend is observed in the case of generative chemical reaction.
(iv) The skin friction coefficient decreased with increasing values of Casson fluid parameter, magnetic parameter and suction parameter, whereas the reverse trend is observed in the case of velocity slip.
(v) The Nusselt number decreases with an increasing the Casson fluid parameter, radiation parameter and thermal slip, where as it increases with an increase in the Prandtl number and the suction parameter.
(vi) The Sherwood number decreases as the Casson fluid parameter, Schmidt number and the solutal slip.

It is hopeful that the present investigation will contribute a better understanding of the flow dynamics and heat and mass transfer of Casson fluid flow over an exponential stretching surface as well as real application.

References

Aziz, E.L. (2009): Viscous dissipation effect on mixed convection flow of a micropolar fluid over an exponentially stretching sheet, Can. J. Phys., Vol. 87, pp. 359-368. https://doi.org/10.1139/P09-047

Bhattacharya, K., Hayat, T. and Alsaedi, A. (2013): Analytic solution for magnetohydrodynamic boundary layer flow of Casson fluid over a stretching/shrinking sheet with mass transfer, Chin. Phys. B, Vol. 22, pp. 024702. https://doi.org/10.1088/1674-1056/22/2/024702

Bhattacharya, K.., Hayat, T. and Alsaedi, A. (2014): Exact solution for boundary layer flow of Casson fluid over a permeable stretching/shrinking sheet, Z. Angew. Math. Mech., Vol. 94, pp. 522-528. https://doi.org/10.1002/zamm.201200031

Bidin, B. and Nazar, R. (2009): Numerical solution of the boundary layer flow over an exponentially stretching sheet with thermal radiation, Eur. J. Sci. Res., Vol. 33, pp. 710-717.

Crane, L. J. (1970): Flow past a stretching plate, Z. Angew. Math. Phys., Vol. 21, pp. 645-647. https://doi.org/10.1007/BF01587695

Dash, R.K., Mehta, K.N. and Jayaraman, G. (1996): Casson fluid flow in a pipe filled with a homogeneous porous medium, Int. J. Eng. Sci., Vol. 34, pp. 1145-1156. https://doi.org/10.1016/0020-7225(96)00012-2

Fang, T., Zhang, J. and Yao, S. (2009): Slip MHD flow over a stretching sheet-an exact solution, Commun. Nonlinear Sci. Numer. Simulat., Vol. 14, pp. 3731-3737. https://doi.org/10.1016/j.cnsns.2009.02.012

Hayat, T., Shehzad, S.A., Alsaediz, A. and Alhothuali, M.S. (2012): Mixed convection stagnation point flow of Cassson fluid with convective boundary conditions, Chin. Phys. Lett., Vol. 29, pp. 114704-1-4. https://doi.org/10.1088/0256-307X/29/11/114704

Hayat, T., Shehzad, S.H. and Alsaed, A. (2012): Soret and Dufour effects on magnetohydrodynamic flow of Casson fluid, Appl. Math. Mech.-Engl. Ed., Vol. 33, pp. 1301-1312. https://doi.org/10.1007/s10483-012-1623-6

Ishak, A. (2011): MHD boundary layer flow due to an exponentially stretching sheet with radiation effect, Sains Malaysiana, Vol. 40, pp. 391-395.

Magyari, E. and Keller, B. (2000): Heat and mass Transfer in the boundary layers on an exponentially stretching continuous surface, J. Phys. D: Appl. Phys., Vol. 32, pp. 577-585. https://doi.org/10.1088/0022-3727/32/5/012

Misra, J.C. and Sinha, A. (2013): Effect of thermal radiation on MHD flow of blood and heat transfer in a permeable capillary in stretching motion, Heat Mass Transf., Vol. 49, pp. 617-628. https://doi.org/10.1007/s00231-012-1107-6

Mukhopadhyay, S. (2013): Casson fluid flow and heat transfer over a nonlinearly stretching surface, Chin. Phys. B, Vol. 22, No. 7, pp. 074701-5. https://doi.org/10.1088/1674-1056/22/7/074701

Mukhopadhyay, S., Prativa Ranjan De, Bhattacharya, K. and Layek, G.C. (2013): Casson fluid flow over an unsteady stretching surface, Ain Shams Eng. J., Vol. 4, pp. 933-938. https://doi.org/10.1016/j.asej.2013.04.004

Mukhopadhyay, S. and Reddy, G.R.S. (2012): Effects of partial slip on boundary layer flow past a permeable exponential stretching sheet in presence of thermal radiation, Heat Mass Transf., Vol. 48, pp. 1773-1781. https://doi.org/10.1007/s00231-012-1024-8

Mustafa, M., Hayat, T., Pop, I. and Aziz, A. (2011): Unsteady boundary layer flow of a Casson fluid due to an impulsively started moving flat plate, Heat Transf. Asian Res., Vol. 40, pp. 563-576. https://doi.org/10.1002/htj.20358

Mustafa, M., Hayat, T., Pop, I. and Hendi, A. (2012): Stagnation point flow and heat transfer of a Casson fluid towards a stretching sheet, Z. Naturforsch., Vol. 67a, pp. 70-76. https://doi.org/10.5560/zna.2011-0057

Nadeem, S., Haq Rizwana, U.I., Akbar, N.S. and Khan, Z.H. (2013): MHD three dimensional Casson fluid flow past a porous linearly stretching sheet, Alexandria Eng. J., Vol. 52, pp. 577-582. https://doi.org/10.1016/j.aej.2013.08.005

Nadeem, S., Haq Rizwana, U.I. and Lee, C. (2012): MHD flow of a Casson fluid over an exponentially shrinking sheet, Sci. Iran. B, Vol. 19, pp. 1550-1553.

Nadeem, S., Rashid, M. and Akbar, N.S. (2014): Optimized analytical solution for oblique flow of a Casson-nano fluid with convective boundary conditions, Int. J. Therm. Sci., Vol. 78, pp. 90-100. https://doi.org/10.1016/j.ijthermalsci.2013.12.001

Nadeem, S., Zaheer, S. and Fang, T. (2011): Effects of thermal radiation on the boundary layer flow of a Jeffery fluid over an exponentially stretching surface, Numer. Algor., Vol. 57, pp. 187-205. https://doi.org/10.1007/s11075-010-9423-8

Pramanik, S. (2014): Casson fluid flow and heat transfer past an exponentially porous stretching surface in presence of thermal radiation, Ain Shams Eng. J., Vol. 5, pp. 205-212. https://doi.org/10.1016/j.asej.2013.05.003

Reddy, P. B. A. (2016): Magnetohydrodynamic flow of a Casson fluid over an exponentially inclined permeable stretching surface with thermal radiation and chemical reaction, Ain Shams Engineering journal, Vol. 7, pp.593-602.

Reddy, P. B. A. and Reddy, N. B. (2011): Thermal radiation effects on hydromagnetic flow due to an exponentially stretching sheet, Int. J. appl. Math. Comp., Vol. 3, pp. 300-306.

Srinivas, S., Reddy, P.B.A. and Prasad, B.S.R.V. (2014): Effects of chemical reaction and thermal radiation on MHD flow over an inclined permeable stretching surface with non-uniform heat source/sink: An application to the dynamics of blood flow, J. Mech. Med. Biol., Vol. 14, pp. 1450067 1-24.